The Footprint of Urban Areas on Global Climate as Characterized by MODIS

Menglin Jin[1], Robert E. Dickinson[2], and Da-Lin Zhang[1]

1: Department of Meteorology
University of Maryland
College Park, MD 20742-2425

2: Earth and Atmospheric Sciences
Georgia Institute of Technology

Submitted to *Journal of Climate*

February 2004

Corresponding author address:

Dr. Menglin Jin
Department of Meteorology
University of Maryland
College Park, MD 20742-2425
Email: mjin@atmos.umd.edu,
Tel.: (301) 405-8833

Abstract

One mechanism for climate change is the collected impact of changes in land cover or land use. Such changes are especially significant in urban areas where much of the world's population lives. Satellite observations provide a basis for characterizing the physical modifications that result from urbanization. In particular, the Moderate Resolution Imaging Spectroradiometer (MODIS) instrument on the NASA Terra satellite measures surface spectral albedos, thermal emissivities and radiative temperatures. A better understanding of these measurements should improve our knowledge of the climate impact of urbanization as well as our ability to specify the parameters needed by climate models to compute the impacts of urbanization. For this purpose, it is useful to contrast urban areas with neighboring non-urban surfaces with regard to their radiative surface temperatures, emissivities, and albedos. Among these properties, surface temperatures have been most extensively studied previously in the context of the "urban heat island" (UHI). Nevertheless, except for a few detailed studies, the UHI has mostly been characterized in terms of surface air temperatures.

To provide a global analysis, we present zonal average of these properties measured over urban areas versus neighboring non-urban areas. Furthermore, we examine individual cities to illustrate the variations of these variables with land cover under different climate conditions [e.g., in Beijing, New York, and Phoenix (a desert city of the United States)]. Satellite-measured skin temperatures are related to the surface air temperatures but do not necessarily have the same seasonal and diurnal variations, since they are more coupled to surface energy exchange processes and less to the overlying atmospheric column. Consequently, the UHI effects from skin temperature

are shown to be pronounced at both daytime and nighttime, rather than at nights as previously suggested from surface air temperature measurements. In addition, urban areas are characterized by albedos much lower than those of croplands and deciduous forests in summer but similar to those of forests in winter. Thus, urban surfaces can be distinguished from non-urban surfaces through use of a proposed index formed by multiplying skin temperature by albedo.

1. Introduction

Large modifications of land surfaces occur often through the development of urban areas. These changes modify local climates (Landesberg 1970, Changnon 1978, 1992). Industrialization and population growth have accelerated this impact through expanded human activities and especially land use. Currently, about 2% of the mid-latitude land is covered by urban and industrial developments (UNPFA 1999, Jin and Zhang 2002). The net effect of buildings and roads over an area is to replace some of the previous natural or managed vegetation with dry impervious surfaces that alter the exchange of energy and moisture between surface and atmosphere, and in doing so modify surface microclimatic variables such as the temperatures, humidity, and near-surface winds.

Because both non-urban and urban surfaces are quite varied, general statements about how they differ are not readily made. Many of the previous studies only examined one or a few selected urban areas (e.g., Bornstern 1968, Karl 1987, 1988, Huff and Vogel 1978, Changnon 1978, Brest 1987, Gallo et. al. 1993, Hansen et al. 2001, Shepherd et. al. 2002). The effects of urbanization vary from city to city. However, temperatures over urban areas are commonly found to be higher than those of outlying rural areas, particularly at night. This elevation of temperatures has been referred to as the "urban heat island" (UHI) (Oke 1982). Urbanization modifies local climates not only through microclimatology, but also through changes in atmospheric radiation and precipitation as initiated by anthropogenic aerosols. These observed changes have been related to land use, building density, population density, and life styles, seasons and prevailing environmental forcing (Oke 1976, 1982; Karl 1988).

Modifications of clouds and precipitation have also been observed over urban landscapes (King et al. 2003, Ramanathen et al. 2001, Shepherd et. al. 2002).

Complementary to such studies are examinations of the role of urbanization on climate from a global perspective as evaluated by IPCC (2001). The present paper is intended to further advance the global perspective of urban impacts on climate. Although relatively small in their area, urban environments are distinguished by being where the bulk of the world's population lives, and where many of the world's climate records are taken. Oke (1976) showed that even for a small town of 1,000 residents, the typical UHI effect is in the range of 2° to 2.5°C. This has recently been confirmed by Torok et al. (2001), who found that the urban-rural temperature differences may scale with the logarithm of a region's population. Such changes can modify mesoscale circulations over urban areas (e.g., Wong and Dirks 1978, Yan and Anthes 1988, Avissar and Pielke 1989, Chen and Dudhia 2001).

Although surface air temperatures observed by World Weather Organization (WMO) have been widely used in the previous UHI studies, changes in sites and instruments as well as irregular coverage (Karl et al.1988, Peterson 2003) complicate this usage. For example, Peterson (2003) found little differences from the urban-rural temperatures detected at 289 stations, and suggested that the urban impact may be at a smaller size than available city and rural stations. Evidently, surface air temperature should be supplemented with other observations to more accurately capture city-induced changes.

Data for skin temperature (T_{skin}) are complementary to those for surface air temperature (T_{air}) (Jin et al. 1997; Jin and Dickinson 1999, 2000, 2002; Jin 2000).

Because of its weaker coupling to the overlying atmosphere, T_{skin} tends to have a stronger UHI signal than T_{air}. We see its UHI for large cities to extend outward from their centers by at least 30 km before becoming undetectable. Nevertheless, the UHI signal from both temperatures varies on daily and seasonal time scales (Roth et. al. 1989).

Urban constructions modify surface properties that contribute to the UHI such as albedo and emissivity. Dense distributions of buildings give a "canyon effect" or "cavity effect", where multiple internal reflections resulting from the urban canopy geometry reduce surface albedo and emissivity from that of individual flat surfaces (Van DeGriend et. al. 1993, Francois et al. 1997, Jin and Liang 2003). Using a model framework to describe the effect of the trapping of insolation by tall buildings, Craig and Lowry (1972) found a 20% decrease in daily albedo.

The effects of urbanization are an example of the land cover/use impact on the climate system. The purpose of this study is to utilize the EOS satellite observations to address the following questions: How significant are the UHI effects over different urban areas in terms of T_{skin}? How do the urban developments affect the land surface physical properties (e.g., albedo and emissivity)? The present study makes a first effort to analyze globally the MODIS land T_{skin}, surface albedo and emissivity.

The next section describes the data sources used for this work. Section 3 presents the evidence of the UHI effects in terms of T_{skin} at the global scale and individual cities, and urban impacts on the surface albedo and emissivity. Section 4 describes a new algorithm that is developed to facilitate the identification of urban areas from satellite observations. Discussion and concluding remarks are given in the final section.

2. Data sources

The Moderate Resolution Imaging Spectroradiometer (MODIS) is carried on NASA's Terra satellite launched in May 2000, and later on the Aqua satellite that is too recent to be used here. On Terra, it measures the earth's surface characteristics through 7 solar and 3 thermal spectral bands at 10:30 LT and 22:30 LT daily. Each pixel has a 1-km resolution at the nadir (Wan and Dozier 1996), and is scaled up to a 5-km resolution in this study. The satellite-measured T_{skin} is derived from longwave bands that detect surface emissions. Its value depends on surface energy budget and so provides an observational constraint on the balance between net surface radiation and fluxes of energy and water (Jin et al. 1997; Jin and Dickinson 1999, 2000). Only the measured values with quality flags attesting to the absence of clouds are used. The MODIS spectral emissivities are converted into broadband values using the MODerate resolution TRANsmittance (MODTRAN) algorithm (see Jin and Liang 2003). The MODIS provisional land-cover product with a 5-km resolution is used herein to categorize the land surface according to the International Geosphere-Biosphere Project (IGBP) 17 land cover types (Friedl et al., 2002), as given in Table 1.

An urban category has not yet been obtained from MODIS observations. As a default, the achieved data uses the Digital Chart of the World urban data that was originally digitized from Operational Navigation and Jet Navigation Charts by the U.S. Defense Mapping Agency (Danko 1992); it is available from the U.S. Geological Survey's EROS Data Center (EDC). Unfortunately, many of the base maps used the urban data from the 1960s and 1970s, and they are inconsistent globally and do not include new cities or new urban development in recent decades (M. Fridel and A.

Schneider, personal communication, 2004; Schneider et al. 2002). Such data could be updated for recent trends in urbanization but do not provide quantitative measures of urban properties that are of importance for climate studies.

A three-parameter, semi-empirical Ross-Thick-Li-Sparse-Reciprocal Bidirectional Reflectance Distribution Function (BRDF) model has been used to characterize the angular dependences of land surface reflectance and the angular integrals giving albedo (Schaaf et al. 2003).

3. Results

In this section, the regional and global occurrences of UHI are first demonstrated using the satellite-measured T_{skin}. Then, surface albedo and emissivity over urban areas are examined to clarify the reasons for the UHI occurrences. Finally, an "urban index" is proposed to identify urban regions using satellite-observed information.

a. The "urban heat island"

The global latitudinal distribution of urban areas and their nocturnal T_{skin} are shown in Fig. 1. Cities are concentrated between 30º - 65ºN in the Northern Hemisphere, with much fewer cities in the tropics and in mid-latitudes in the Southern Hemisphere where the earth surface is mostly covered by water. Significant longitudinal variations in urban T_{skin} are seen corresponding to the north-south distribution of net radiation received at the earth surface. In this figure, cloud contamination is minimized through the use of clear days. Thus, the indicated variability of T_{skin} depends on factors such as variation in absorption of solar radiation, variation in elevation, nearness of oceanic influences, and dryness of the underlying surfaces. The largest range at 30ºN of more than 30°C occurs where the largest fraction of land is covered by deserts.

On average, the urban T_{skin} are 1 - 5°C higher than those over croplands, with larger differences during nighttime in the Southern (winter) Hemisphere (Fig. 2b). By comparison, the daytime T_{skin} differences between the urban areas and adjacent croplands are small but still detectable, especially in the range of 10°S – 40°N and 30 - 45°S (Fig. 2a). Cities at high latitudes in the Northern Hemisphere (e.g., 55 - 60°N) are even cooler than the rural areas during daytime. Large T_{skin} differences are also notable at the desert latitudes of 15 - 25°N and 10 - 20°S because T_{skin} in desert cities are close to those in their surrounding deserts but higher than those in their nearby croplands. A large drop in urban T_{skin} occurs near 15° N at which latitude few cities are located. The amplitude of diurnal T_{skin} changes is small (<10°C) in the tropics and Southern Hemisphere where oceanic influences are most pronounced, whereas it is large (> 30°C) at middle to high latitudes in the Northern Hemisphere.

The differences between the urban and forest regions over subtropical and middle latitudes of the Northern Hemisphere are about 4°C (Fig. 3) with extremes up to 12°C at around 22°N. Urban differs more from forests during the day than it is at night.

Three examples of major cities are examined in this study, namely, two large metropolitan cities in developed and developing countries (i.e., New York and Beijing) and one city with extreme natural (desert) condition (i.e., Phoenix, Arizona). As shown in Fig. 4a, the city of Beijing is surrounded mostly by cropland, except to its west (cf. Fig. 4a and Table 1); its northwest to southeast orientation reflects its urban expansion to Tianjin, which is one of the most rapidly growing coastal cities in China. High skin temperatures are evident over Beijing during both the daytime and nighttime of January and July (see Figs. 4b and 4c). The MODIS data show more pronounced UHI effects

over the southern part of the city where its building density is higher than that over its northern part with its more widely spaced buildings such as universities, research institutions and government offices, as well as parks and lakes. The "*Weekly Weather & Crop Bulletin*" shows for this month little rainfall across most of the Northern China Plain, including the Beijing metropolitan area. Presumably more irrigation than normal was needed as a response, possibly amplifying the daytime urban-rural contrast at that time and so weakening the day-night contrasts (cf. Figs. 4c,d). The July nighttime T_{skin} of Beijing was only elevated with respect to the eastern cropland but not relative to the western forest mountains (see Fig. 4d).

To exclude the influence of the latitudinal variation of solar insolation at different latitudes, Fig. 5 compares urban T_{skin} longitudinally to the adjacent rural areas over a spatial scale of 200 km for the city of New York. Its UHI effects are visible in January during both daytime and nighttime (cf. Figs. 5a,b). New York, as an east-coastal city, has relatively small diurnal changes of T_{skin}, as compared to Beijing, but it is warmer than the adjacent pixels to the west during both the daytime and nighttime. The nocturnal T_{skin} decreases steeply going inland in winter, e.g., as much as 5°C across the 200-km range, whereas in daytime or in summer, there is a more flat change of about 2°C.

Because the city of Phoenix, the 17th largest city of the U.S., has more vegetation than its surrounding areas, its T_{skin} is substantially lower during both the day and nighttime (see Figs. 6a,b). The coldest pixel to the west of the city (i.e., 314 K by day and 296 K at night) occurs over local mountains. But its UHI effects are barely detectable in January for either day or night.

b. Urban effects on surface albedo and emissivity

Urban construction reduces both albedo and emissivity (Figs. 7a, b). Figure 7a compares the zonal averaged urban albedo to the averaged cropland albedo between 30° and 65°N, where most cities are located. City albedo values are 2 - 5% smaller than those in the adjacent croplands, as noted earlier, e.g., by Brest (1987). The largest urban albedos are observed over the desert areas around 30°N and accompanied by high daytime and nighttime T_{skin} (see Fig. 6). Surface emissivity is about 1 – 2% lower than that of nearby croplands (Fig. 7b). The spatial distributions of albedo and emissivity for Beijing are given in Fig. 8, which shows that the southern part of the city has albedo lower than 0.12, and emissivity lower than 0.94, i.e., 3% less than the emissivity of the surrounding regions.

Albedo is determined by MODIS as a weighted average of spectral albedos at 7 different wavelengths. For use in climate models, they are divided into visible and near-infrared wavelengths. Further insights are provided herein as to the difference between urban and non-urban areas and how it is distributed spectrally through Figs. 9, 10 and 11, using the city of New York as an example. The longitudinal distribution of total albedo is compared in Fig. 9 with its component visible and near-infrared broadbands, which indicates that the urban and non-urban difference is largely from the near-infrared differences. This distinction is further seen from Fig. 10 that shows averages over the urban area versus nearby cropland and deciduous forest. Two differences are evident: (a) the relative changes in the near-infrared are larger than in the visible (about 25% versus about 10%), and (b) the near-IR albedo is nearly an order of magnitude larger than the visible albedo. In other words, the urban and rural visible albedos are both

about 0.04, whereas the urban near-infrared albedo is 0.27 compared to about 0.32 for cropland and forest. The shortwave broadband albedo, which is approximately an average of the visible and near-infrared broadband albedos, is about 0.15 for urban and 0.18 for cropland and forest.

Figure 11 presents the spectral variations of albedo and the contrasts between winter and summer. We have only sampled snow-free and cloud-free pixels, and thus the seasonality is largely from changes in the sun angle, browning and drop of leaves and more exposure of bare soil. In general, urban albedo varies significantly with wavelength, with higher albedo in NIR and lower albedo in the visible in both July and January. In July, the peak difference occurs at 0.9 μm, with an urban value of 0.34 and cropland and forest values higher than 0.4. In January, the contrasts are smaller and the peak difference occurs at 1.2 μm.

4. The urban index

Urban areas have generally been determined from satellite data from the nighttime lighting. Such a measure is more an index of electricity use than of the urban features that are significant for climate study. For such purpose, indices are needed that are related to the mechanisms by which urban areas modify climate. We find that urban areas can usefully be characterized by combining skin temperature and albedo (α_i), i.e.,

$$UI_i = (1 - \alpha_i)*T_{skin-i} \quad (1)$$

where UI represents the urban index, and the subscript 'i' denotes each pixel.

Figure 12 compares the UHI structures of New York and its surrounding regions analyzed using T_{skin} to those using the UI. Because of their large T_{skin}, the cities of New York, Washington, D.C., and Philadelphia are already well identified from the T_{skin} map

(see Fig. 12a). However, as shown for Phoenix, some urban areas have similar T_{skin} to their surrounding rural regions so that T_{skin} alone is not a reliable index. With the UI, the three eastern US urban areas are easily detected by higher UI values than their neighboring non-urban regions. Similarly, the urban index for Beijing shows a more realistic size and spatial spread of Beijing than its original MODIS land cover data (cf. Figs. 4a and 13).

Thus, the UI provides a physically-based urban mapping approach to distinguishing urban from rural areas. Further development using the general principals behind the index presented here should eventually provide a robust, well validated measure of urban intensities from the viewpoint of climate modeling.

5. Discussion and Concluding Remarks

In this study, the EOS satellite-measured skin temperatures are used to identify globally the urban areas in order to evaluate the human impact on the earth's climate system. The UHI effects are found in terms of skin temperature anomalies both locally for a few selected cities and globally, and in all seasons and at both the daytime and nighttime. Previous studies emphasized the UHI effects in terms of surface air temperature at night during summer when surface winds are light.

In this paper, we have shown through a global analysis of satellite data that T_{skin} is mostly but not always larger in urban than in surrounding rural areas. Urban areas have a wide variety of surfaces including many of those present in the rural areas. Thus, it is not possible to make generalization that compares all urban with all rural areas. However, cities are distinguished by their large fraction of mostly dark impervious areas, often asphalt. These surfaces introduce into urban environments distinctly higher

Bowen ratios and lower albedos and emissivities. These surfaces may typically be up to 0.3 or more for densely populated areas. The daytime sensible heat fluxes of moist areas are typically less than half of the latent fluxes, so with a large impervious fraction, the sensible fluxes and hence the daytime boundary layer warming may be nearly doubled. With higher Bowen ratios, the fraction of net daytime radiation being stored is also comparably larger leading to warmer nighttime temperatures. This fraction of impervious area is the primary distinction between urban and forest surfaces, which indeed have overall albedos slightly lower than urban ones. Shorter vegetation has higher and smoother albedos, amplifying their diurnal range from that of the rougher cities and forests, since their atmospheric surface boundary layers respond with larger temperature gradients for the same daytime heating and nighttime cooling. Their albedo difference overall makes them cooler than urban areas, but concentrated at night when the effect of surface roughness is additive rather than canceling the albedo difference (being realized to some degree at night through less storage of the rural surface). Our examination of Beijing illustrated the differences from the urban region with both nearby forests and croplands.

Most UHI studies have been in moist mid-latitude cities. In dry regions, the Bowen ratios are generally larger in the rural areas as the cities have more vegetation, and the effects described above are reversed. However, the urban areas will have compensating lower albedos. Our analysis of Phoenix indicates little distinction between the city and its surroundings, possibly a general result for semi-arid and arid regions.

The MODIS results presented herein have important implications with respect to the modeling of land-surface processes for climate change. Specifically, high-resolution

satellite observations of the surface albedo, emissivity and land cover could be used to update the land surface parameters for both numerical weather prediction and global (regional) climate models (e.g., Jin and Liang 2003). The effect of urban areas on the regional climate system occurs through the land surface-atmosphere interactions. Beside the effects described here, urban areas are known to modify the distribution of aerosol, clouds, and rainfall (King et. al. 2003). Climate models may provide a good approach for assessing the global consequences of the urban climate modifications.

Acknowledgements

We would like to thank Dr. Zhengmin Wan and Dr. Feng Gao for their kindly preparing the MODIS land surface data for this study. Special thanks go to Dr. Michael D. King of NASA/Goddard Space Flight Center for his helpful discussions on the MODIS reflectance and albedo retrieval, and to Eva Wong of the Environmental Protection Agency for sharing information of UHI studies. This work was funded by NASA's EOSIDS project.

REFERENCES

Avissar, R., and R.A. Pielke, 1989: A paremeterization of heterogeneous land surfaces for atmospheric numerical models and its impact on regional meteorology. *Mon. Wea. Rev.,* **117**, 2113-2136.

Bornstern, R. D., 1968: Observations of the urban heat island effect in New York city. *J. Appl. Meteor*., **7**, 575-582.

Brest, C. L., 1987: Seasonal albedo of an urban/rural landscape from satellite observations. *J. Clim. Appl. Meteor*., **26**, 1169-1187.

Changnon, S. A. Jr., 1978: Urban effects on severe local storms at St. Louis. *J. Appl. Meteor.*, **17**, 578-592.

——, 1992: Inadvertent weather modification in urban areas: Lessons for global climate change. *Bull. Amer. Meteor. Soc*., **73**, 619-627.

Chen, F., and J. Dudhia, 2001: Coupling an advanced land surface-hydrology model with the Penn State – NCAR MM5 modeling system. Part II: Preliminary model validation. *Mon. Wea. Rev*., **129**, 587-604.

Craig, C. D., and W. P. Lowry, 1972: Reflections on the urban albedo. *Preprints, Conf. on Urban Environ. and 2nd Conf. on Biometeor.*, Amer. Meteor. Soc., Philadelphia, 159-164.

Danko, D. M., 1992: The Digital Chart of the World project. PE & RS, **58**,1125-1128.

Francois, C., C. Ottle, and L. Prevot, 1997: Analytical parameterization of canopy directional emissivity and directional radiance in the thermal infrared. Application on the retrieval of soil and foliage temperatures using two directional measurements. *Int. J. Remote Sensing,* **18**, 2587-2621.

Friedl, M. A., D. K. McIver, J. C. Hodges, Y. Zhang, D. Muchoney, A. H. Strahler, C.E. Woodcock, S. Gopal, A. Schneider, A. Cooper, A. Baccini, F. Gao, and C.B. Schaaf, 2002: Global land cover mapping from MODIS: Algorithms and early results. *Remote Sensing Environ*., **83**,287-302.

Gallo, K. P., A. L. Mcnab, T. R. Karl, J.F. Brown, J.J. Hood, and J. D. Tarpley, 1993: The use of NOAA AVHRR data for assessment of the urban heat island effect. *J. Appl. Meteor*., **32**, 899-908.

Hansen, J., R. Ruedy, M. Sato, M. Imhoff, W. Lawrence, D. Easterling, T. Peterson, and T. Karl, 2001: A closer look at United States and global surface temperature change. *J. Geophy. Res.*, **106** (D20), 23,947-23,963.

Huff, F. A., and J. L. Vogel, 1978: Urban, topographic and diurnal effects on rainfall in the St. Louis region. *J. Appl. Meteor*., **17**, 565-577.

IPCC 2001: *The Intergovernmental Panel on Climate Change, Climate Change 2001: The Scientific Basis*. Cambridge University Press. 881pp.

Jin, M., 2000: Interpolation of surface radiation temperature measured from polar orbiting satellites to a diurnal cycle. Part 2: Cloudy-pixel Treatment. *J. Geophys. Res.*, **105**(D3), 4061-4076.

——, R.E. Dickinson, and A. M. Vogelmann, 1997: A Comparison of CCM2/BATS Skin Temperature and Surface-Air Temperature with Satellite and Surface Observations. *J. Clim.*, **10**, 1505-1524.

——, and ——, 1999: Interpolation of surface radiation temperature measured from polar orbiting satellites to a diurnal cycle. Part 1: Without clouds. *J. Geophys. Res*., **104**, 2105-2116.

——, and ——, 2000: A Generalized algorithm for retrieving cloudy sky skin temperature from satellite thermal infrared radiances**.** *J. Geophys. Res.***, 105**(D22), 27,037-27,047.

——, and D.-L. Zhang, 2002: Changes and interactions between skin temperature and leaf area index in summer 1981-1998. *Meteor. Atmos. Phys.,* **80**, 117-129.

——, and R. E. Dickinson, 2002: New observational evidence for global warming from satellite, *Geophys. Res. Lett*., **29**(10), 10.1029/2001GL013833.

——, and S. Liang, 2003: Improve emissivity parameter in land surface model using MODIS observations. Conditionally accepted by *J. Climate*.

Karl, T. R., and C. N. Willams, Jr., 1987: An approach to adjusting climatological time series for discontinuous inhomogeneities. *J. Clim. Appl. Meteor*., **26**, 1774-1763.

——, H. F. Diaz, and G. Kukla, 1988: Urbanization: Its detection and effect in the United States Climate Record. *J. Climate*, **1**, 1099-1123.

King, M. D., W. P. Menzel, Y. J. Kaufman, D. Tanré, B. C. Gao, S. Platnick, S. A. Ackerman, L. A. Remer, R. Pincus, and P. A. Hubanks, 2003: Cloud and aerosol properties, precipitable water, and profiles of temperature and humidity from MODIS. *IEEE Trans. Geosci. Remote Sens.*, **41**, 442-458.

Landsberg, H. E., 1970: Man-made climatic changes. *Science*, **170**, 1265-1274.

Oke, T. R., 1976: City size and the urban heat island. *Atmos. Environ.,* **7**, 769-779.

——, 1982: The energetic basis of the urban heat island. *Quart. J. R. Meteor. Soc*., **108**, 1-24.

Peterson, T. C., 2003: Assessment of urban versus rural in situ surface temperatures in the contiguous United States: No difference found. *J. Climate,* **16,** 2941-2959.

Ramanathan, V., P. J. Crutzen, J. T. Kiehl, and D. Rosenfeld, 2001: Aerosols, climate, and the hydrological cycle. *Science*, **294**, 2119-2124.

Roth, M. T. R. Oke, and W. J. Emery, 1989: Satellite-derived urban heat islands from three costal cities and the utilization of such data in urban climatology. *Int. J. Remote Sensing*, **10**,1699-1720.

Schaaf, C. B., and Co-authors, 2003: First Operational BRDF, Albedo and Nadir Reflectance Products from MODIS. *Remote Sens. Environ.* In press.

Schneider, A., M. A. Friedl, D. K. McIver, and C. E. Woodcock, 2002: Mapping urban areas by fusing multiple sources of coarse resolution remotely sensed data. *Photogramm. Eng. Remote Sens*., **69**, 1377-1386.

Shepherd, J. M., H. Pierce, and A. J. Negri, 2002: Rainfall modification by major urban areas: Observations from spaceborne rain radar on the TRMM satellite. *J. Appl. Meteor*., **41**, 689-701.

Torok, S. J., J. G. Morris, C. Skinner, and N. Plummer, 2001: Urban heat island features of southeast Australian towns. *Australian Meteorol. Mag.*, **50**, 1-13.

UNPFA, 1999: *The State of World Population 1999*. United Nations Population Fund, United Nations Publications, 76pp.

Van DeGriend, A. A. Van, and M. Owe, 1993: One the relationship between thermal emissivity and the normalized difference vegetation index for nature surfaces. *Int. J. Remote Sensing*, **14**, 1119-1131.

Wan, Z., and J. Dozier, 1996: A generalized split-window algorithm for retrieving land-surface temperature from space. *IEEE Trans. Geo. Remote Sens*., **34**, 892-904.

Wong, K. K., and R. A. Dirks, 1978: Mesoscale perturbations on airflow in the urban mixing layer. *J. Appl. Meteor*., **17**, 677-688.

Yan, H., and R.A. Anthes, 1988: The effect of variation in surface moisture on mesoscale circulations. *Mon. Wea. Rev*., **116**, 192-208.

Table 1: Global land-cover index from http://geography.bu.edu/landcover/userguidelc/consistent.htm.

Land cover index
1. Evergreen Needleleaf
2. Evergreen Broadleaf
3. Deciduous Needleleaf
4. Deciduous Broadleaf
5. Mixed Forest
6. Closed Shrubland
7. Open Shrubland
8. Woody Savanna
9. Savanna
10. Grasslands
11. Permanent Wetlands
12. Cropland
13. Urban
14. Cropland/Natural Veg
15. Snow and Ice
16. Barren
17. Water

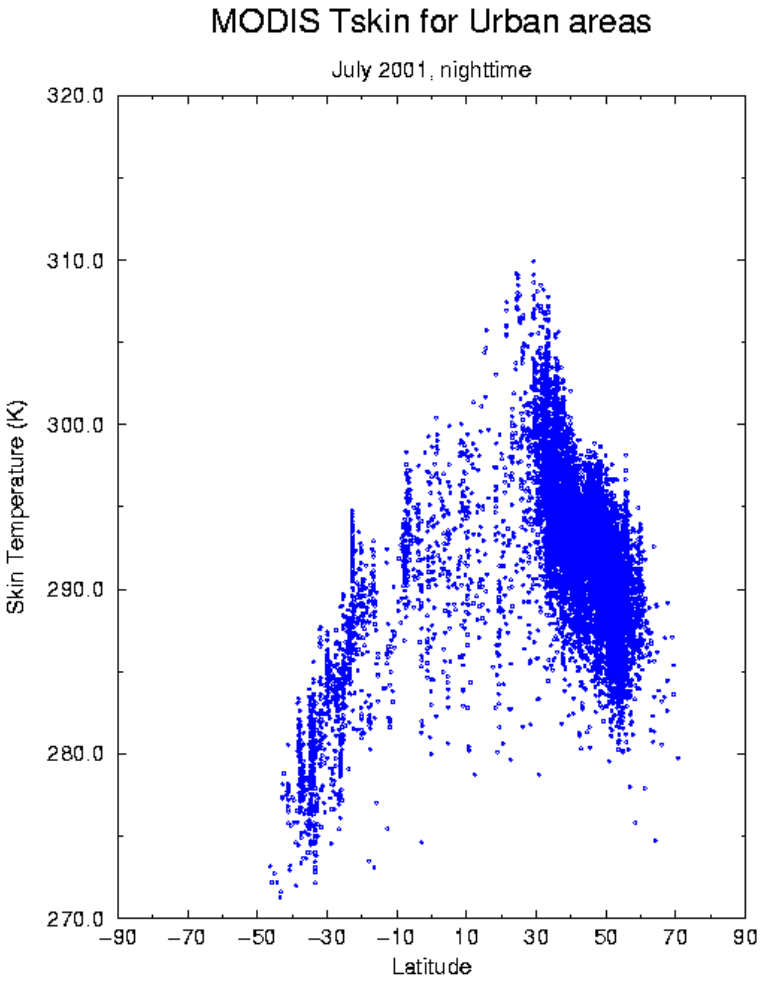

Figure 1. Longitudinal variation of monthly mean nocturnal urban skin temperatures for the month of July 2001. Urban areas are obtained from the USGS data, while skin temperatures are obtained from the MODIS data at a 5-km resolution.

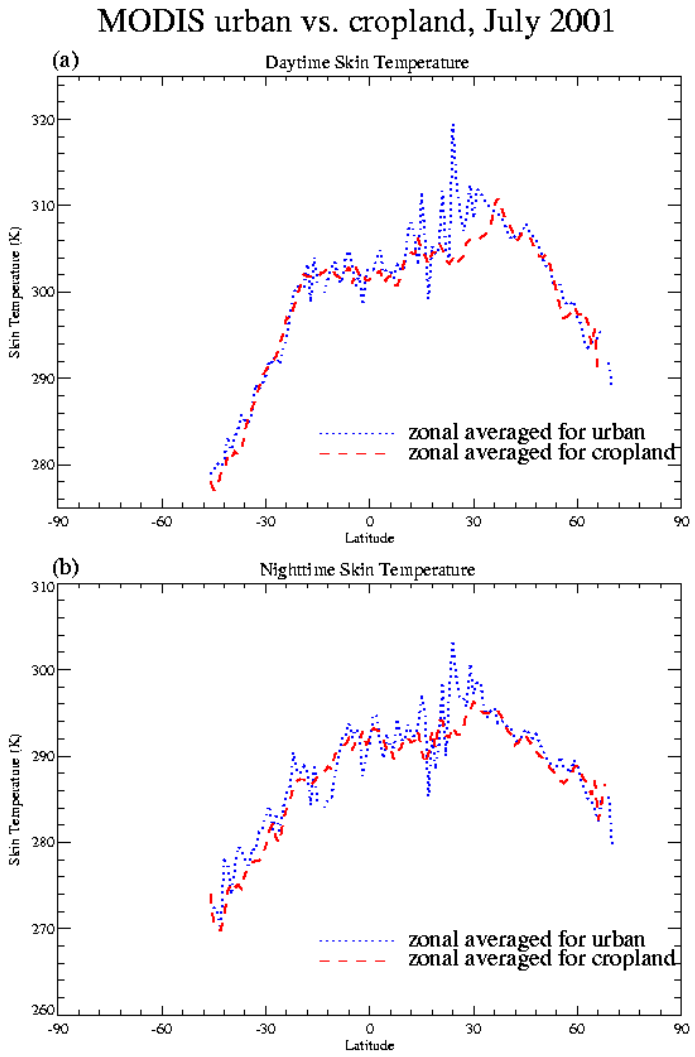

Figure 2: Comparison of the monthly and zonal averaged skin temperatures between the urban surfaces and surrounding croplands: (a) daytime, and (b) nighttime, for the month of July 2001.

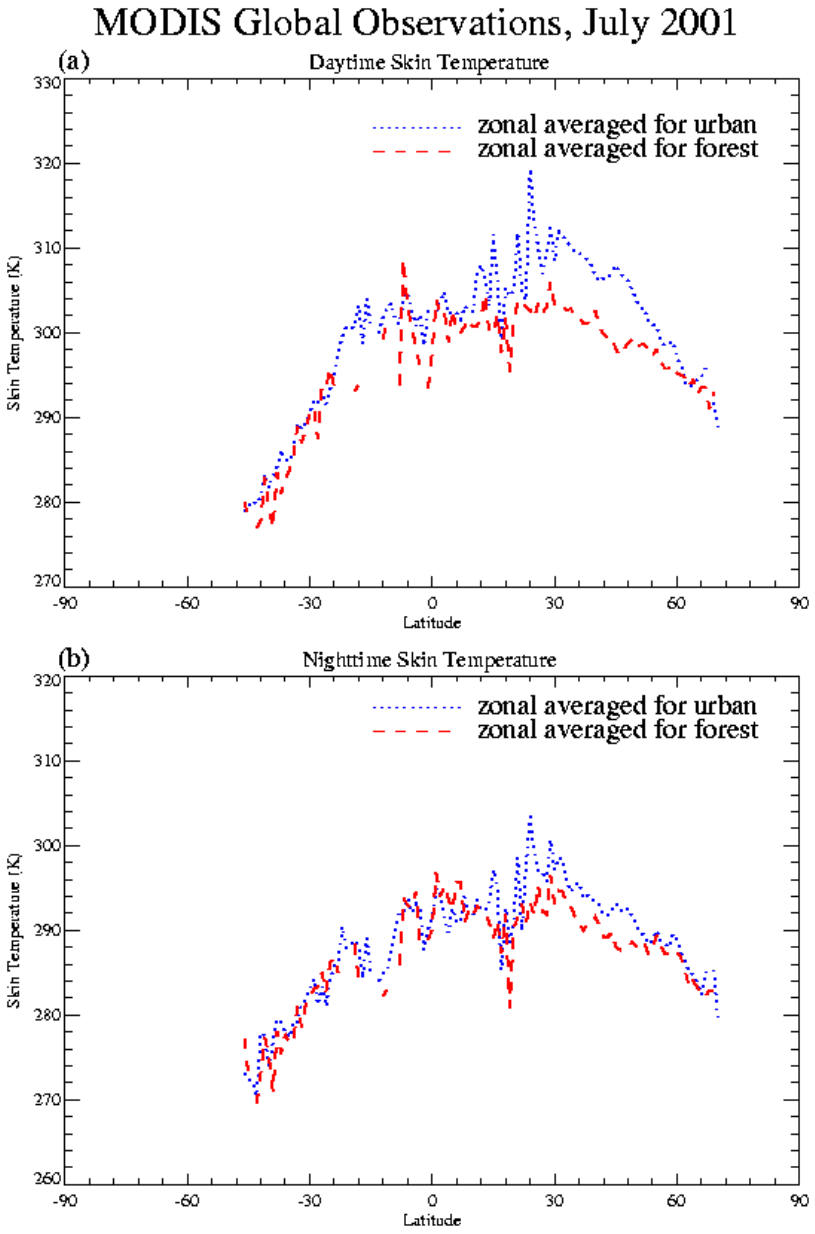

Figure 3. Comparison of the monthly and zonal averaged skin temperatures between the urban surfaces and surrounding forests: (a) nighttime; and (b) daytime for the month of July 2001. The forests are nearby (100 km) of the urban regions.

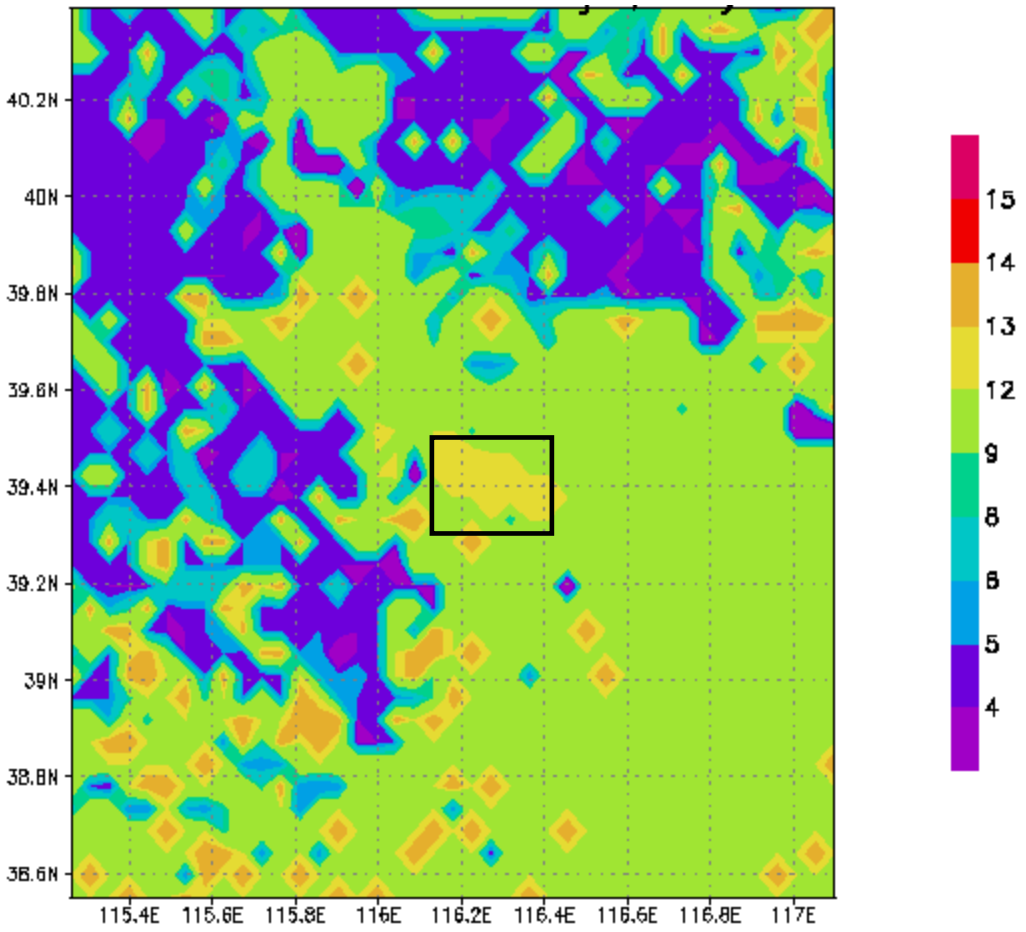

Figure 4 (a) Horizontal distribution of the land-cover indices (see Table 1) over Beijing and its neighboring area that is obtained from the MODIS land-cover product. Each grid is 5 x5 km.

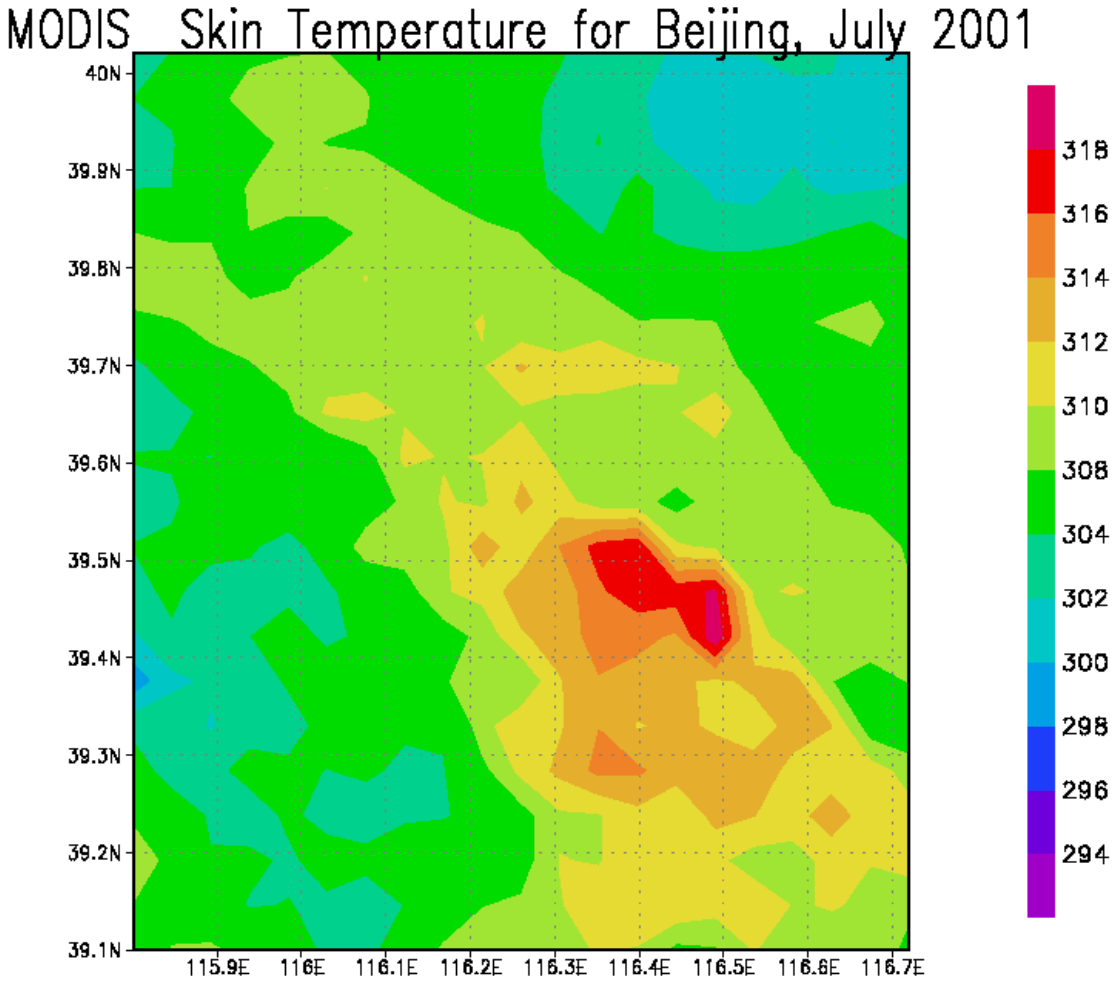

Figure 4 (b) Horizontal distribution of the monthly mean daytime skin temperature (in Kelvin) over Beijing and its surroundings for the month of July 2001.

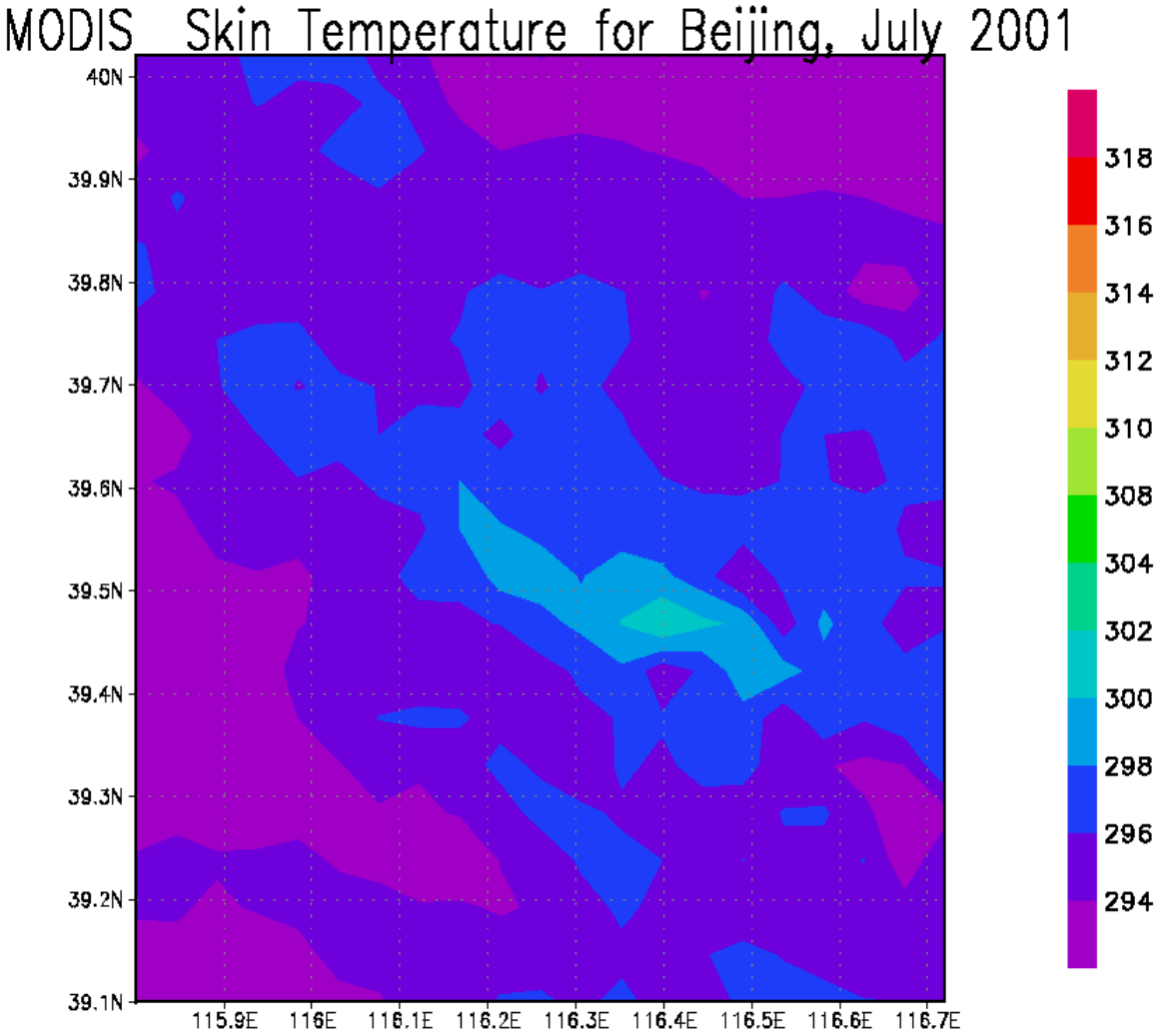

Figure 4 (c) As in (b) but for the night-time skin temperature.

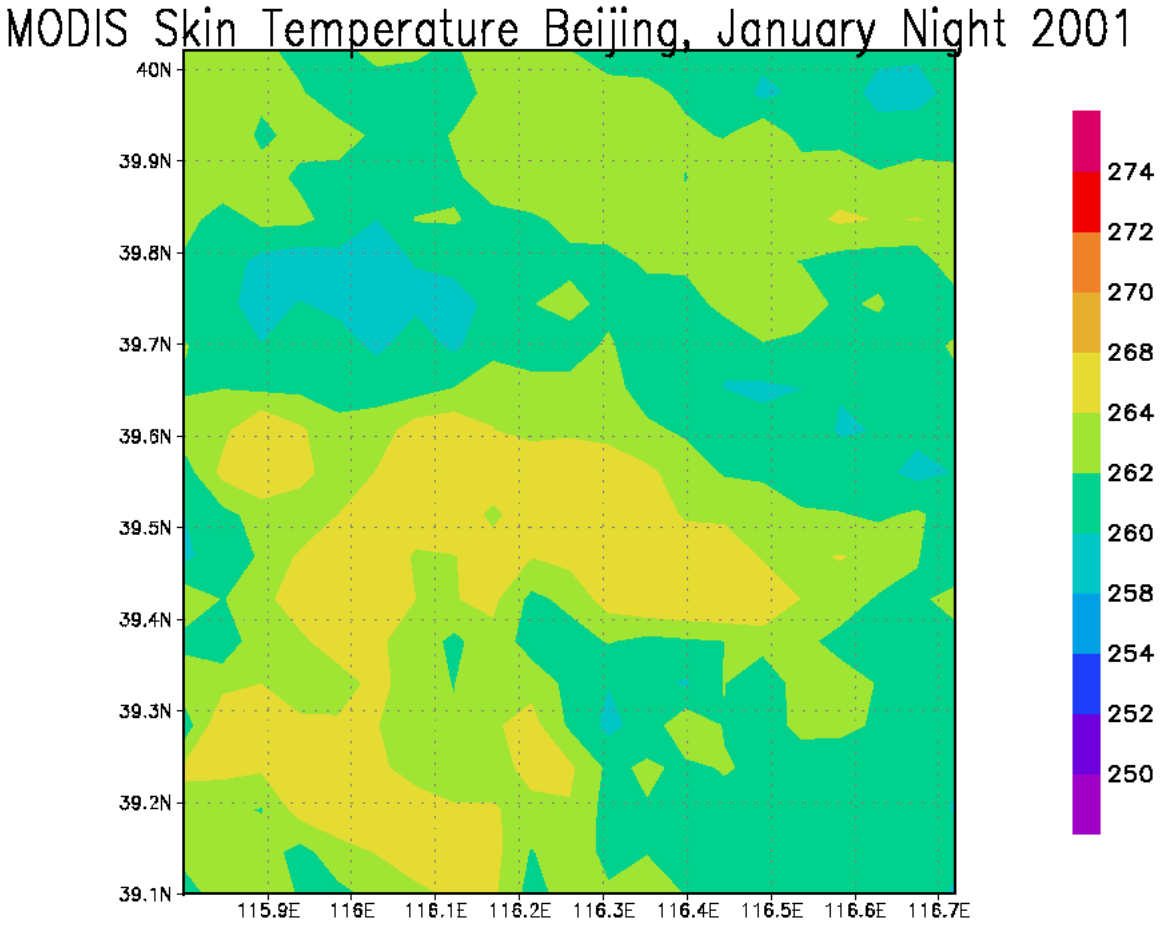

Figure 4 (d) As in (b), but for the nighttime skin temperature for the month of January 2001.

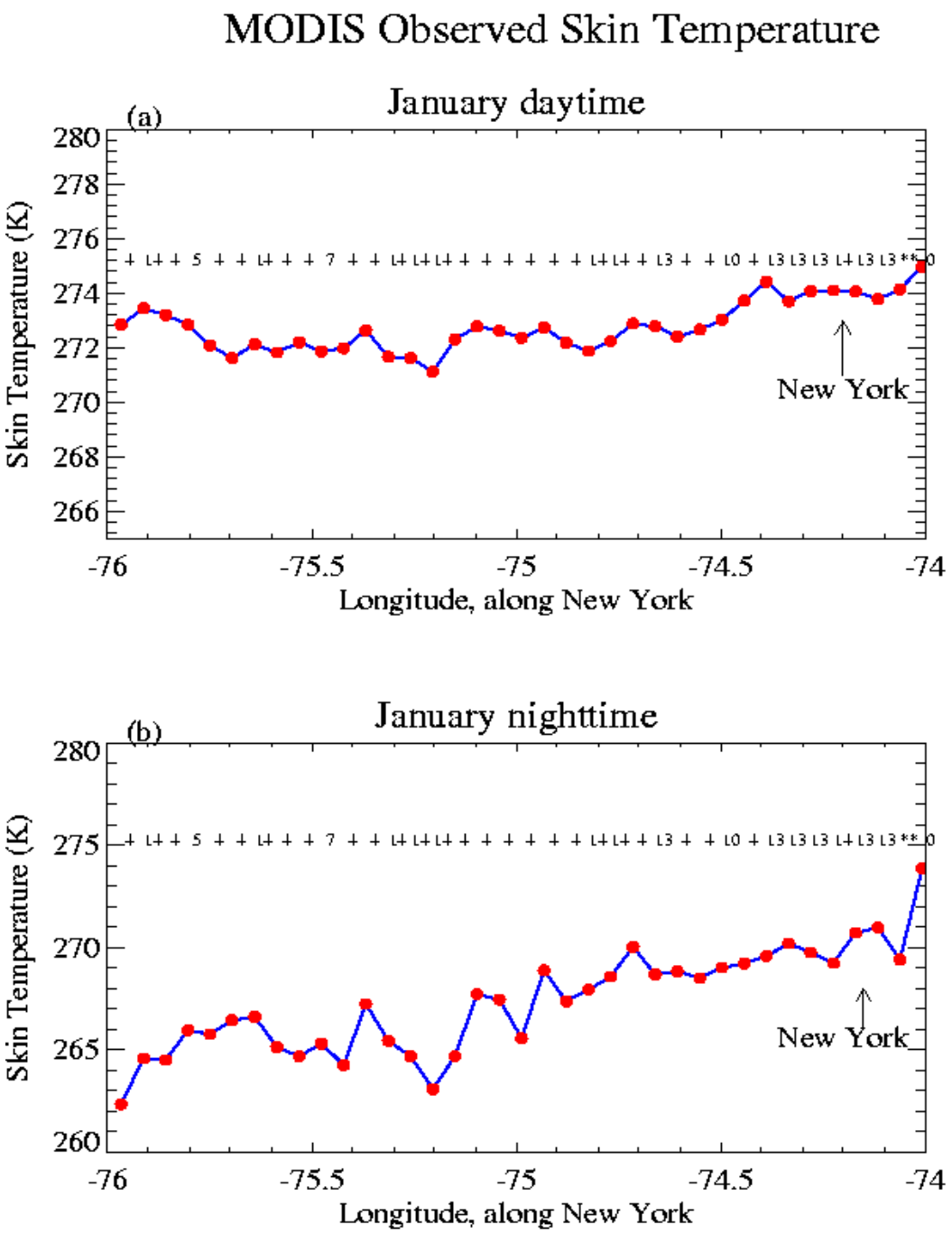

Figure 5. The zonal distribution of monthly-averaged skin temperatures and land cover for each pixel through the latitude of the New York city: (a) daytime; and (b) nighttime for the month of January 2001. Land cover information for each pixel (at 5 km) is given as Ascii values in the plot. Index of 13 denotes the urban coverage; See Table 1 for the definition of other land-cover indices.

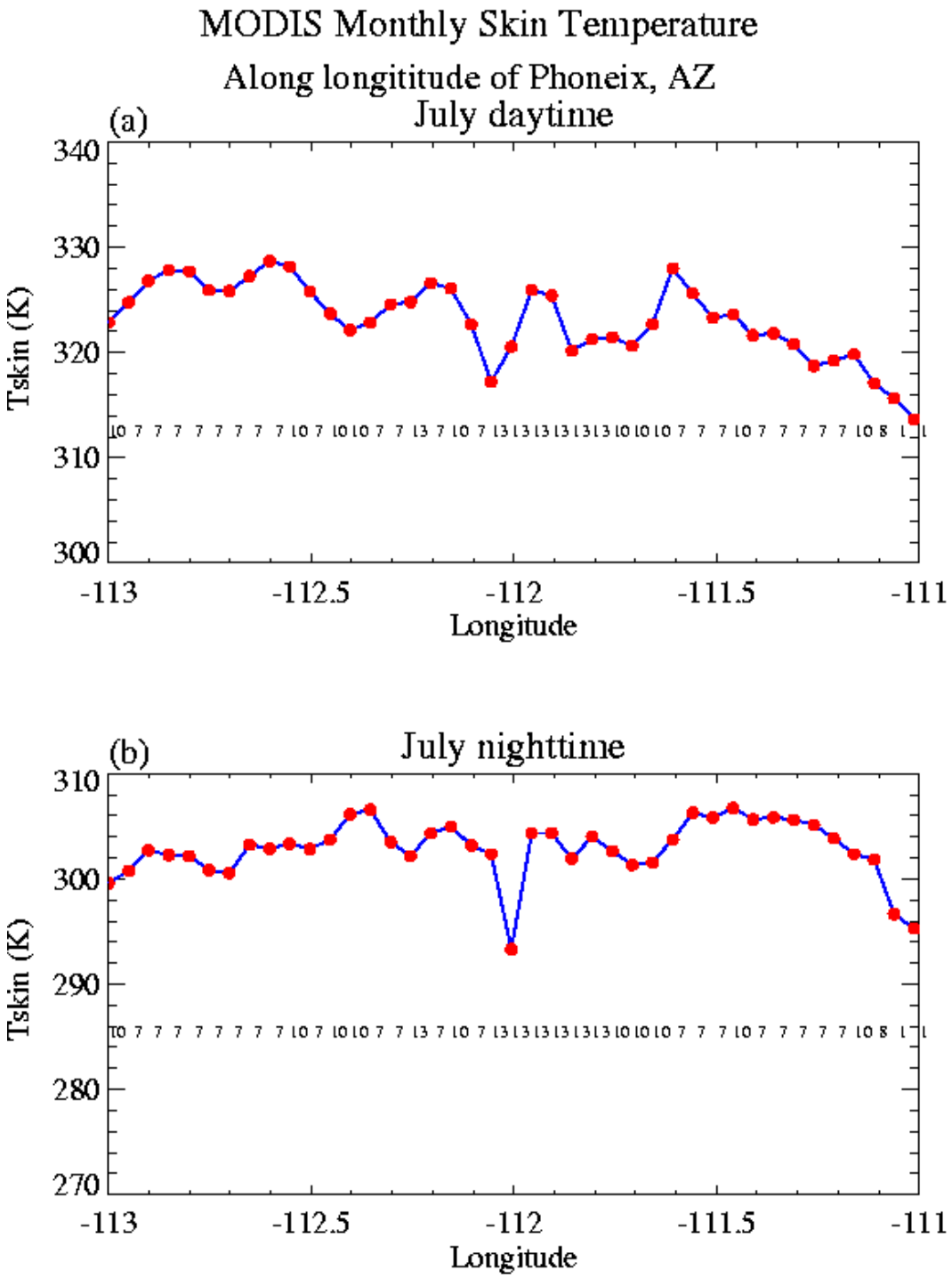

Figure 6. As in Fig. 5 but for Phoenix, Arizona.

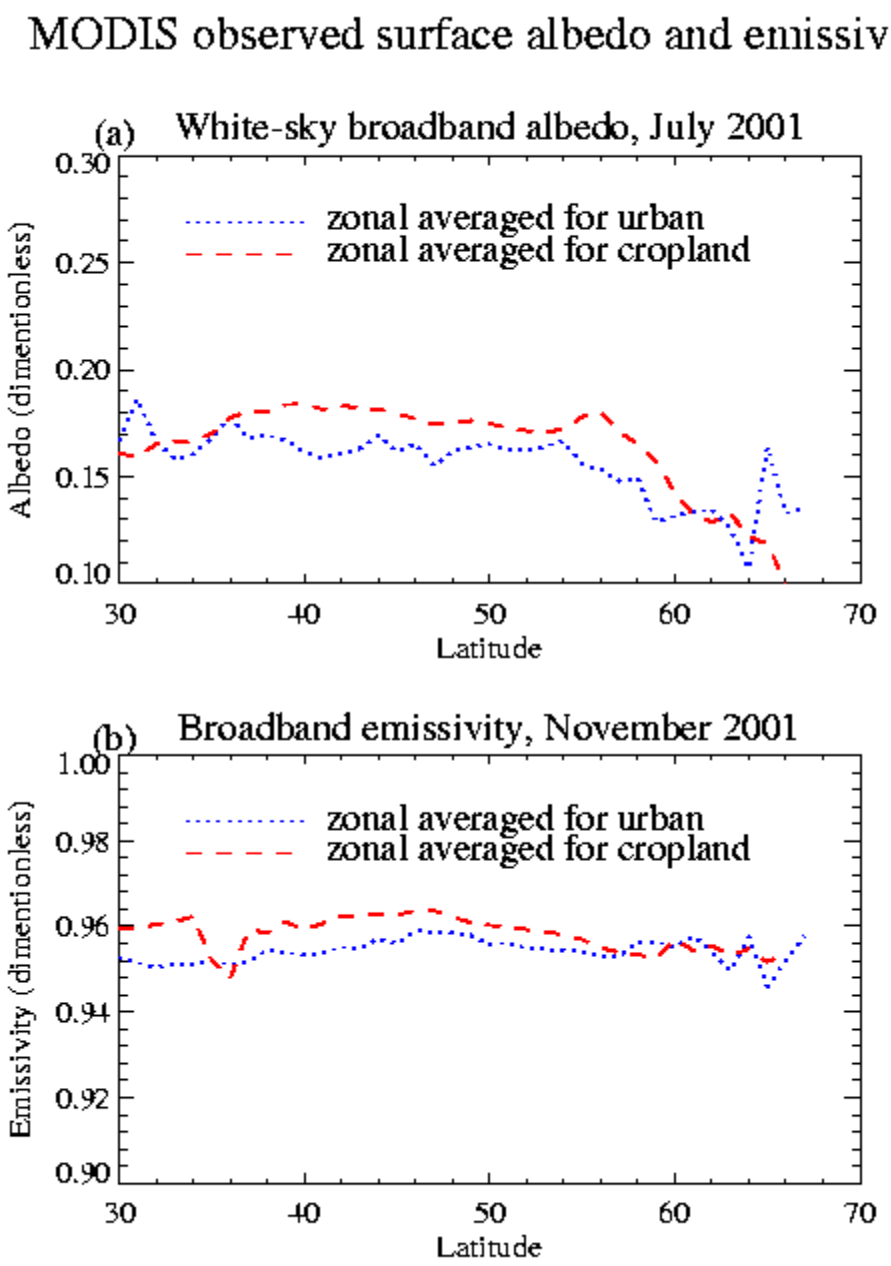

Figure 7. Monthly and zonal averaged (a) surface albedo for the month of July 2001; and (b) surface emissivity for the month of November 2001 in the latitudes of 30 - 70°N over urban areas (dotted lines) and their adjacent croplands (dashed lines).

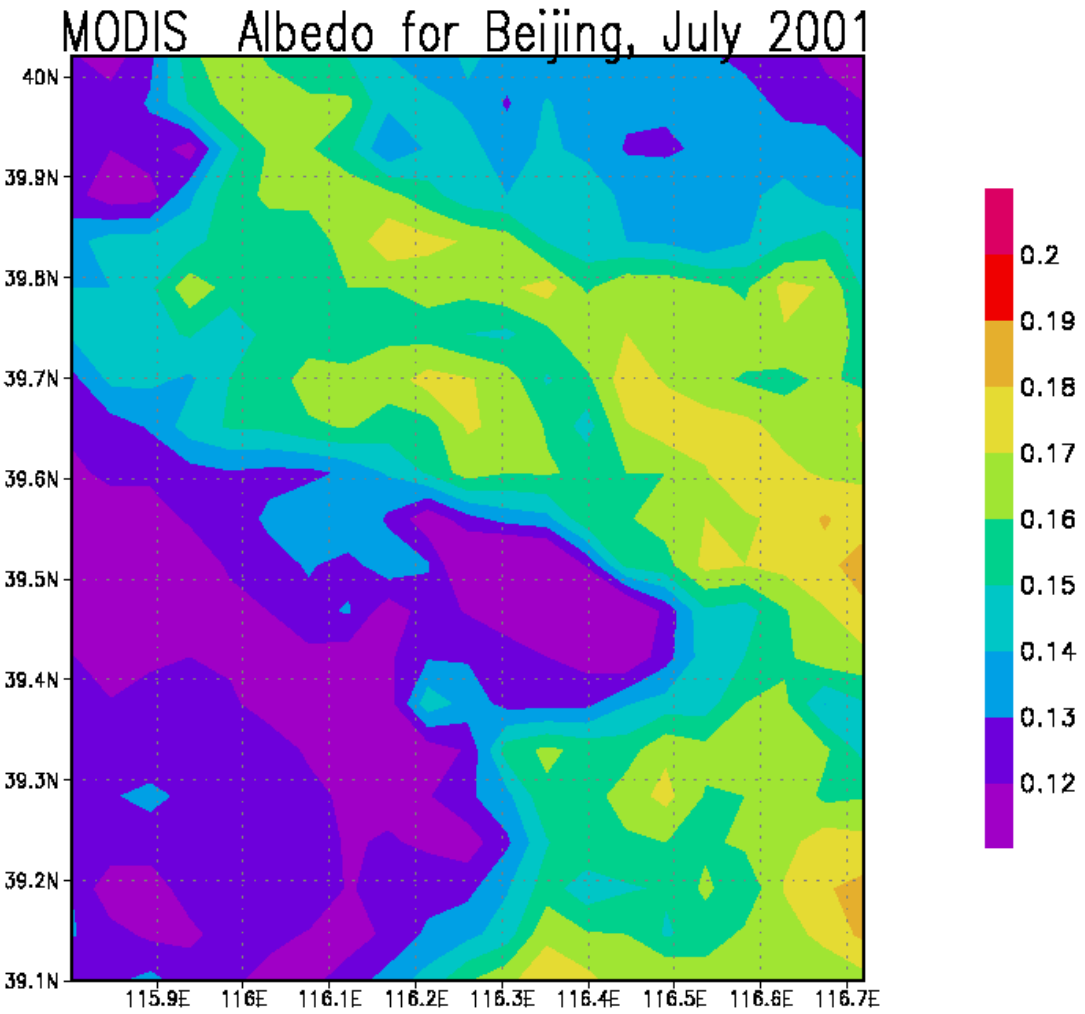

Figure 8a. Spatial variation of the monthly mean surface albedo over Beijing and its surroundings for the month of July 2001.

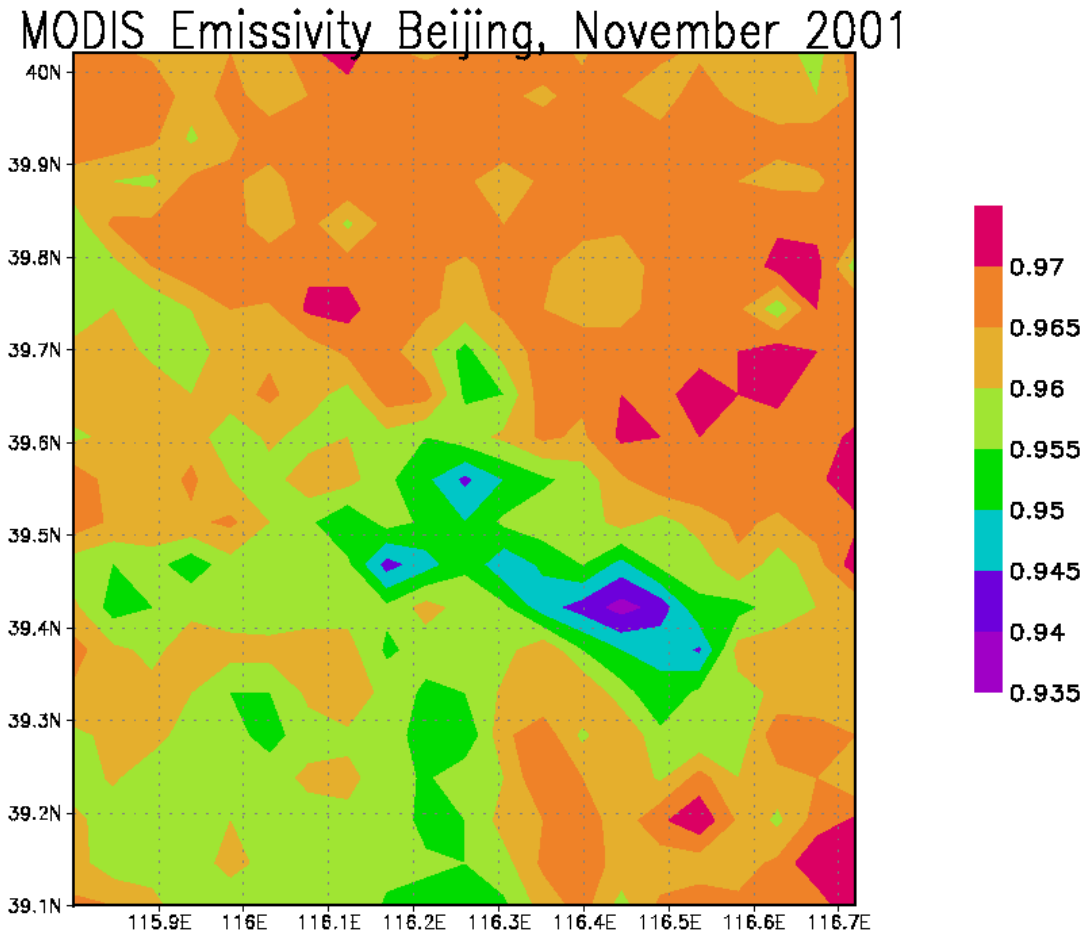

Figure 8b. Spatial distribution of the monthly mean surface emissivity over Beijing and its surroundings for the month of November 2001.

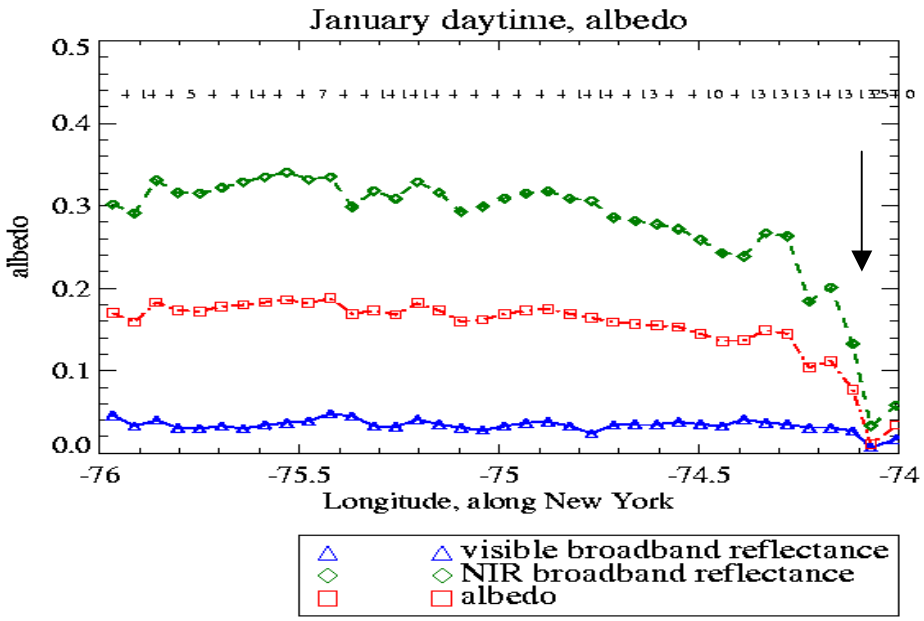

Figure 9. As in Fig. 5 but for the surface shortwave, near-infrared and visible broadband albedos. The arrows link the urban pixels (category 13) with the corresponding abrupt decrease on reflectance.

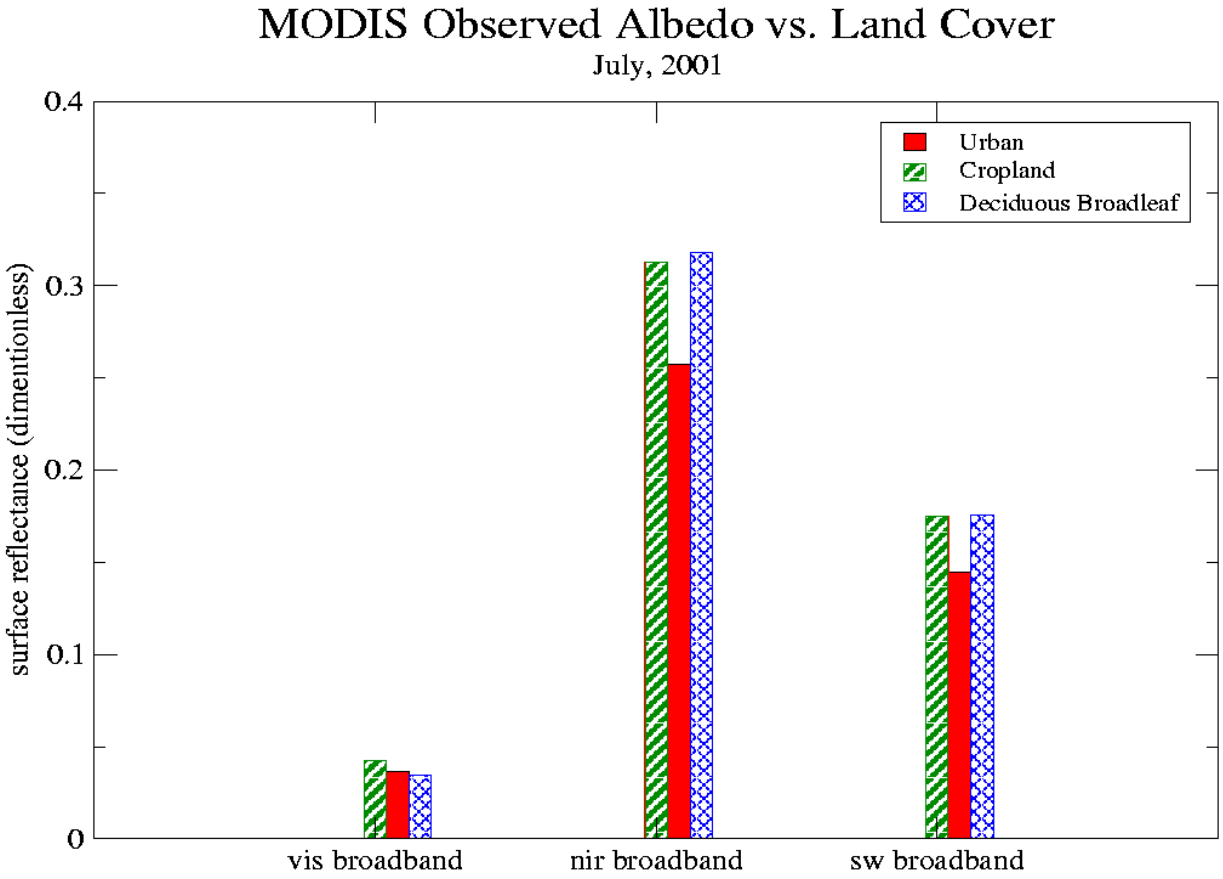

Figure 10: Comparisons of visible broadband (vis), near infrared broadband (nir) and showtwave broadband (sw) albedos for urban, cropland, and deciduous broadleaf land cover over New York and surrounding regions.

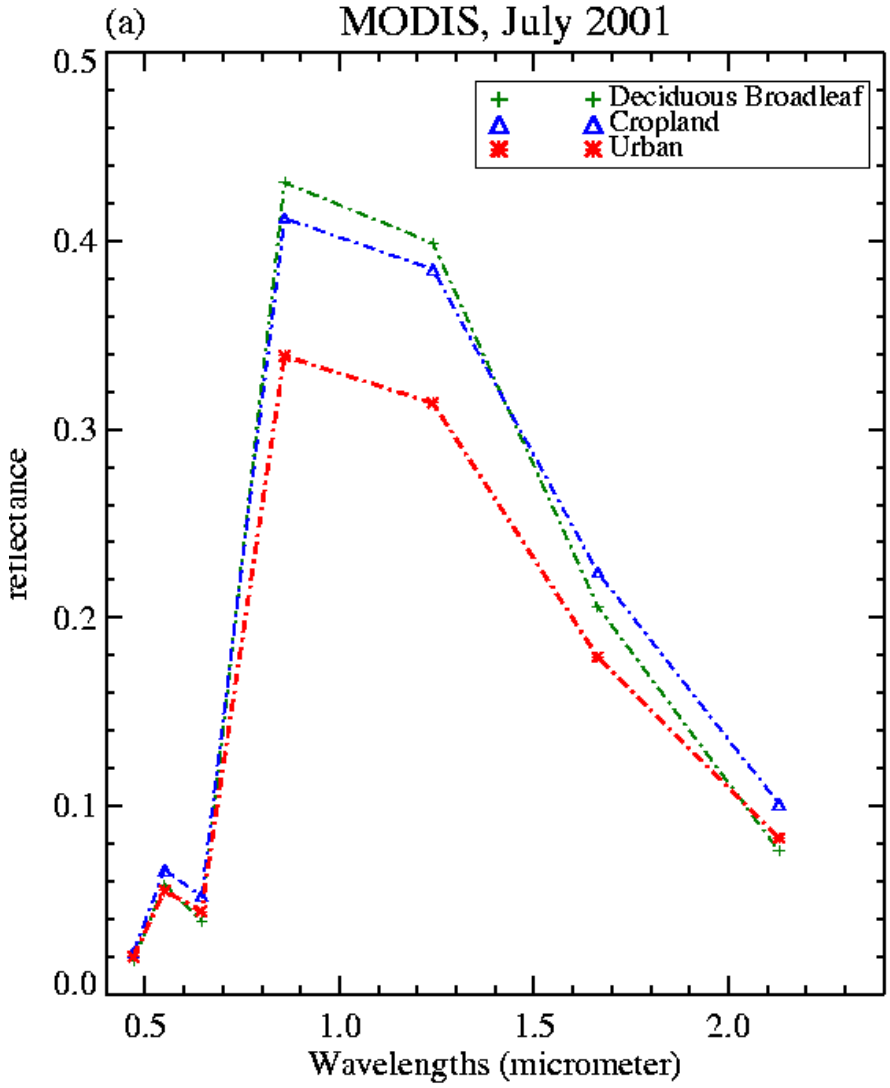
(a)
MODIS, July 2001
Deciduous Broadleaf
Cropland
Urban
reflectance
0.0
0.1
0.2
0.3
0.4
0.5
0.5
1.0
1.5
2.0
Wavelengths (micrometer)

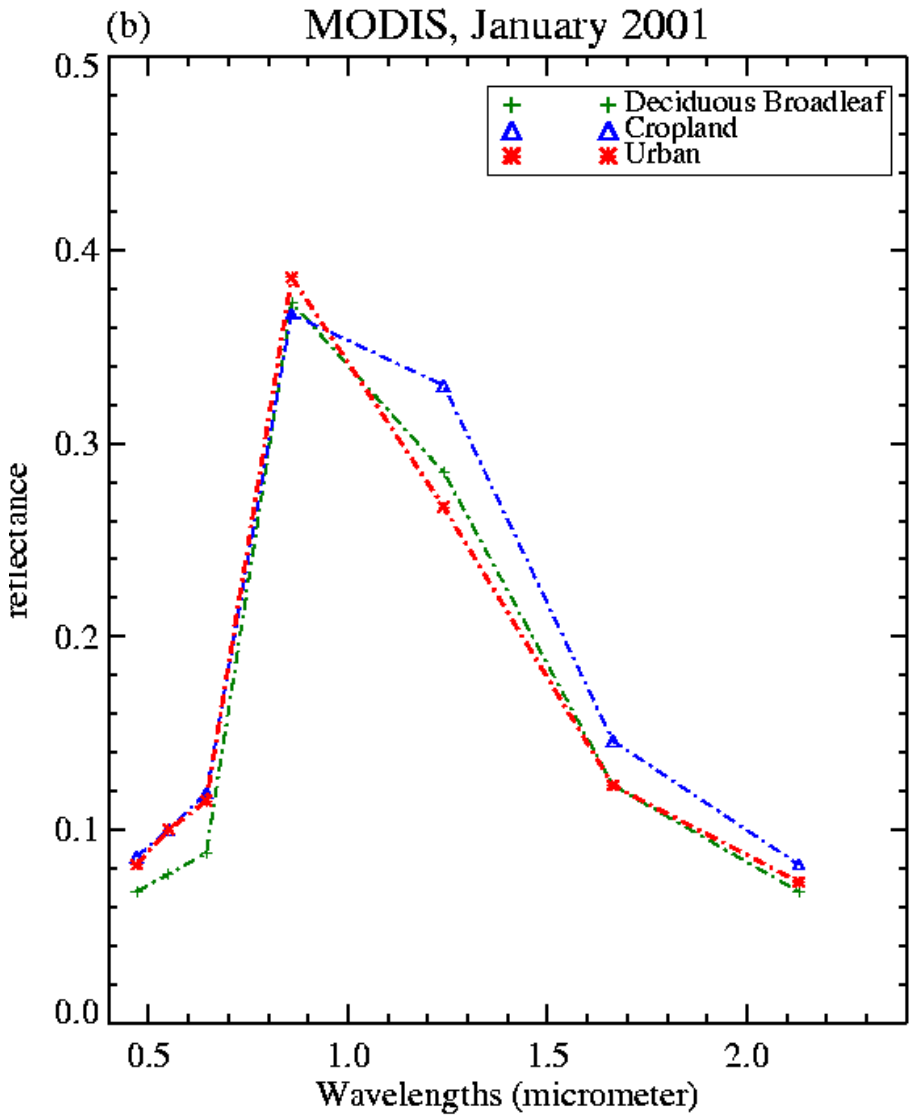

Figure 11: The spectral albedo for urban, cropland, and deciduous broadleaf from MODIS, for New York and surrounding regions, as in Figures 10 and 12. (a) is for July and (b) is for January.

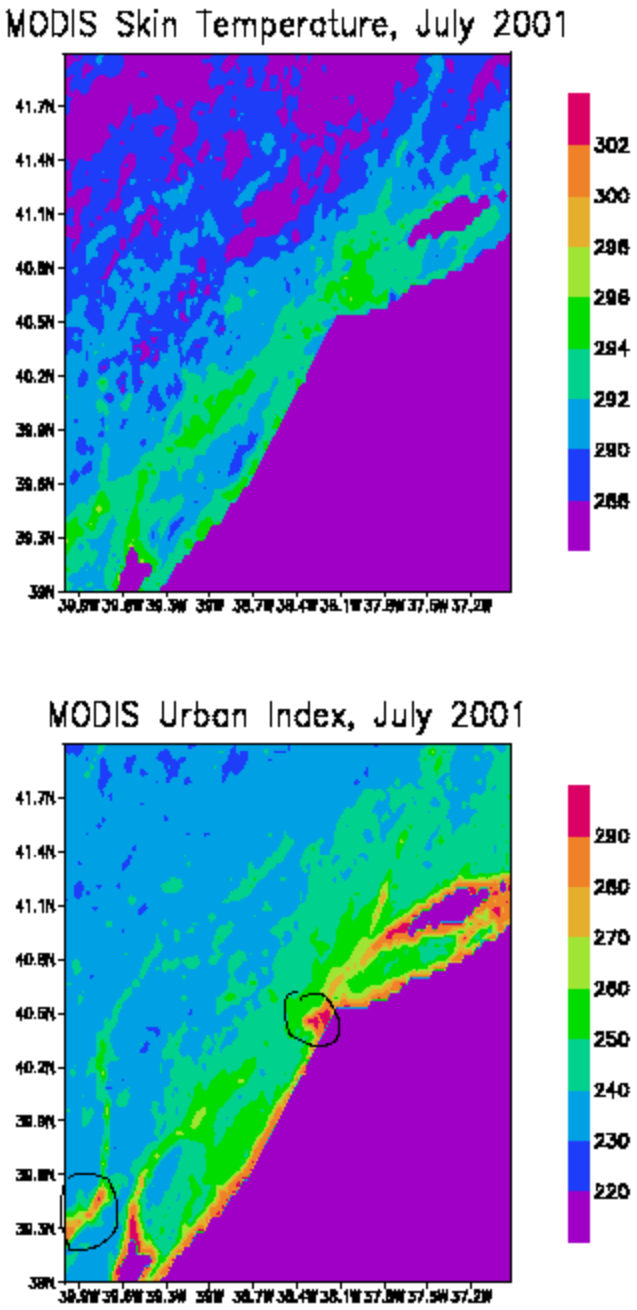

Figure 12. Urban index for July 2001 for New York and its surrounding areas: (a) skin temperature, and (b) the corresponding urban index. The circled areas in (b) show better the urban characteristics of New York and Washington, D.C. than those in (a).

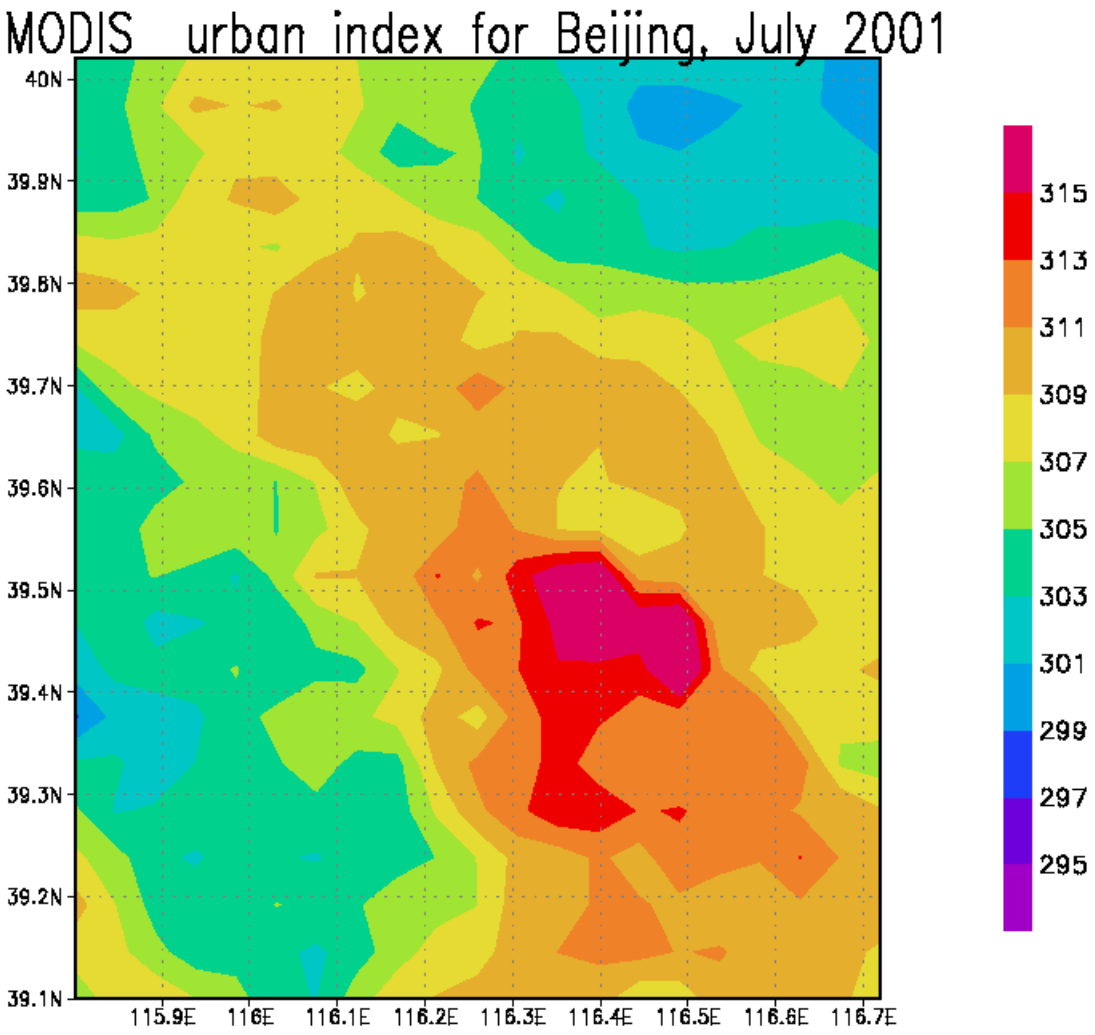

Figure 13. Urban index over Beijing and its surrounding areas for the month of July 2001.